The Astrophysical Journal, 585:1007–1014, 2003 March 10

ι CASSIOPEIAE: ORBIT, MASSES, AND PHOTOMETRY FROM ADAPTIVE OPTICS IMAGING IN THE I AND H BANDS[1]

Jack Drummond, Scott Milster, and Patrick Ryan
Starfire Optical Range, Directed Energy Directorate, Air Force Research Laboratory, Kirtland Air Force Base, NM 87117-5776

and

Lewis C. Roberts, Jr.
The Boeing Company, 535 Lipoa Parkway, Suite 200, Kihei, HI 96753
Received 2002 February 15; accepted 2002 November 20

ABSTRACT

The multiple-star system ι Cas was observed as a calibration for our adaptive optics observations in 2001 July with the Advanced Electro-Optical System (AEOS) 3.63 m telescope in Maui, Hawaii, and the first ever image of the faint astrometric component Aa (along with A and B) was obtained at the H-band wavelength. Another image was obtained in 2002 February with the same telescope, but that time in the I band. This wider image includes the C component and is the first to show four components. By combining our images with seven recent speckle interferometry measurements, a 47 yr period relative orbit is derived for the A-Aa components. Comparing the motion of B with respect to the A-Aa system, previous A-B orbits are rejected in favor of simple rectilinear motion of B across the field. Nevertheless, the history of the relative vector separation between B and A reveals the suborbital motion of A around its center of gravity with Aa, leading to a true orbit for A. The masses of A and Aa are thus determined to be 1.99 ± 0.28 and $0.69 \pm 0.12\ M_{\odot}$, respectively. Combining our differential photometry in the I and H bands with B and V information from the Tycho-2 catalog, we derive spectral types for all four from their colors: component A is spectral type A3 with peculiar red colors, Aa is G6, B is F5, and C is K3.

Subject headings: binaries: visual — instrumentation: adaptive optics — stars: fundamental parameters — stars: individual (ι Cassiopeiae) — techniques: high angular resolution

1. INTRODUCTION

As part of our search for faint companions around stars using a coronagraph (Ryan et al. 1998; Ryan, Drummond, & Milster 2002) with adaptive optics (AO) on the Advanced Electro-Optical System (AEOS) 3.63 m telescope (Roberts & Neyman 2002) on Haleakala on the island of Maui, we observed ι Cas in 2001 July in the H band as a calibration standard for orientation and image scale. Without using the coronagraph, we obtained images showing three components. A fourth, C, was just outside our 4″ field of view, and a fifth, D, is 211″ away. Component D is not addressed here. While the faint component Aa has long been known to exist from its effect on the A-B pair for over 170 years (see Heintz 1996) and was first detected with speckle interferometry in 1982 (McAlister et al. 1987), Figure 1 is the first image of Aa. Another, wider field image that includes the C component was obtained in 2002 February in the I band. Figure 2 is the first image showing the four components. The ι Cas system is also known as STF 262 AB, WDS 02291+6724, HD 15089, ADS 1860 AB, HR 707, HIP 11569, Tycho 4058-1504-1 and 4058-1504-2 (components A and B), and Tycho 4058-1505-1 (component C).

2. OBSERVATIONS AND ANALYSIS

2.1. *H Band*

At 12:17 UT on 2001 July 25, while gathering data for calibration, we obtained several 1 s closed-loop images of ι Cas through an astronomical H-band (1.65 μm) filter with a NICMOS camera set up in one of the AEOS coudé laboratories. Ten 1 s images were sky-subtracted and averaged. Because an aberration produced by a misalignment in the AO optical train (which was corrected later in the night) was so prominent during this time, we modified the parametric blind deconvolution (PBD) point-spread function (PSF) of Drummond (1998; Barnaby et al. 2000) to include four Gaussians around the Lorentzian plus Airy pattern core. Initially, each star was required to have the same pattern, scaled by the intensity for the star, which is appropriate for stars within an isoplanatic patch. However, the residuals indicated that the strict isoplanatic assumption was not valid, and so the isoplanatic assumption was relaxed by requiring each PSF to have the common four-Gaussian aberration and Airy pattern but allowing them to have individual Lorentzian shapes. A more thorough discussion is given by Drummond et al. (2002).

A nonlinear least-squares program solves for the common Gaussians, the individual central Lorentzians, and the common central Airy, as well as the individual positions and intensities. Figure 1 shows the data with the aberration and Lorentzians subtracted, leaving behind what should be Airy patterns, and Figure 3 shows mesh plots of the system and the model subtractions. Because the data are fitted with least squares, uncertainties in all of the parameters are determined simultaneously. Quantities of interest are given in Table 1, where the uncertainties in the magnitude differences are propagated from the uncertainties in the least-squares parameters and include covariances among the parameters. On the other hand, the formal fitting uncertainties for the position angles and separations are so small that their uncertainties in the table are due exclusively to calibration uncertainties.

[1] Based on observations made at the Maui Space Surveillance System operated by Detachment 15 of the US Air Force Research Laboratory's Directed Energy Directorate.

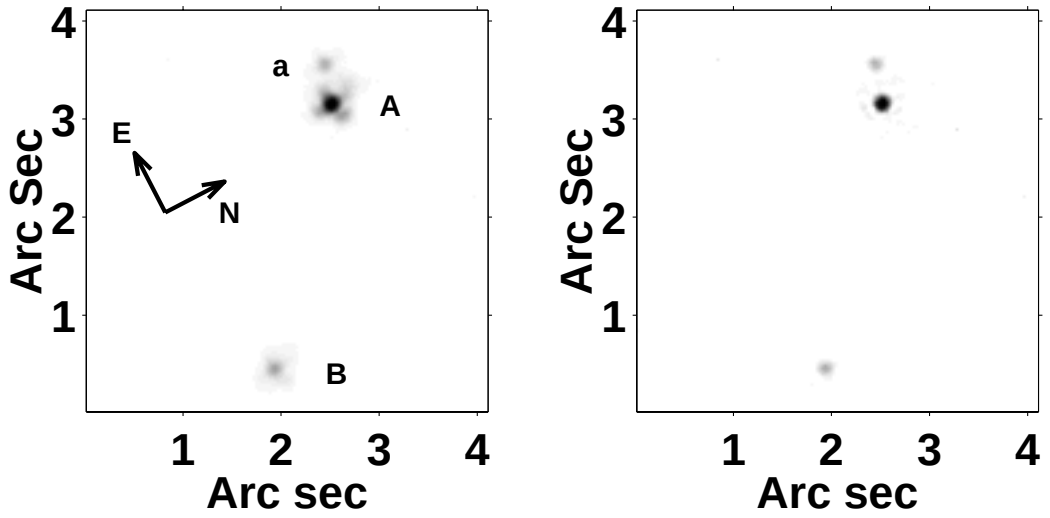

FIG. 1.—Image of ι Cas at 1.65 μm. Three components of ι Cas are clearly separated with AO on the 3.63 m AEOS telescope on Haleakala on 2001 July 25. This is the first time the small astrometric/spectroscopic companion Aa has been imaged. *Left*: Sky-subtracted image showing the strong optical aberration pattern around each star. *Right*: Image with the common aberration and individual Lorentzian cores subtracted off, leaving hints of Airy patterns. Both are displayed on a square root scale. The size of the Lorentzian component in B compared to A and Aa indicates that the field is not isoplanatic.

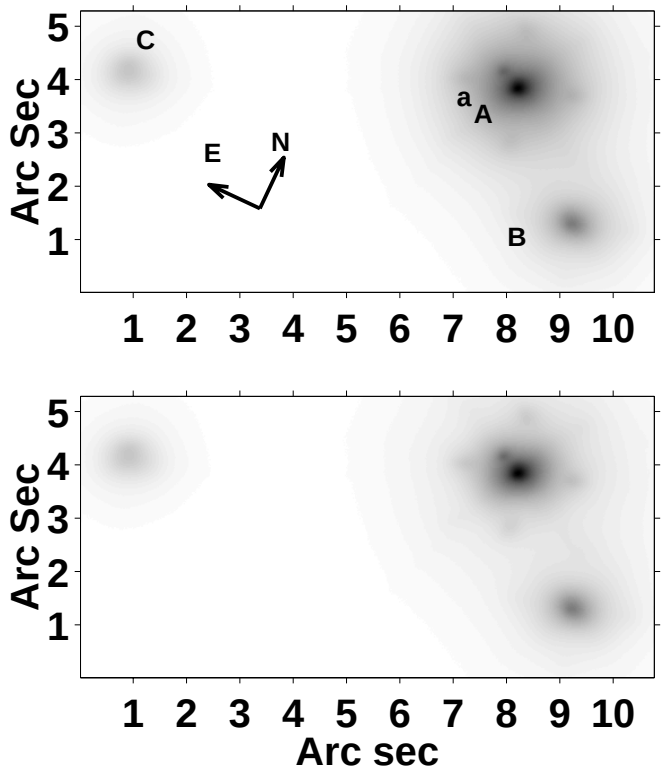

FIG. 2.—Image of ι Cas at 0.9 μm. Four components of ι Cas are clearly separated with AO on the 3.63 m AEOS telescope on Haleakala on 2002 February 21. This is the first image showing all four components. *Top*: Sky-subtracted image, which, unlike in Fig. 1, is displayed on a log scale in order to show the faint C component. *Bottom*: Also on a log scale, the image with the common Gaussian subtracted off, leaving the different-sized Lorentzian cores, indicating that, except for A and Aa, the stars are not within the same isoplanatic patch (see text). In addition, because it is not modeled, the characteristic AO waffle pattern can be seen around A/Aa as four faint spots.

2.2. *I Band*

At 6:32 UT on 2002 February 21, we obtained another set of images, this time with the standard science camera of the AEOS AO system in the *I* band (0.9 μm). There were 1000 frames collected, with exposure times of 0.4 s. The frames were bias- and dark-subtracted and flat-fielded. Saturated frames were thrown out, and the remaining 359 frames were co-added after being shifted to a common center. Because the object was at 33° elevation, the AO performance was somewhat degraded. Since the AO system's science camera has a larger field of view (10.″2) than the coudé room mounted IR camera that was used in 2001, the C component was captured in the image, Figure 2. Figure 4 is a mesh plot of the image, and Figure 5 is a close-up showing the Aa component on the shoulder of A. For PBD of the *I*-band image, the PSF was found to be composed of a central Lorentzian on top of a broad Gaussian, with no sign of either the Airy pattern or the aberration visible in the *H*-band images. As in the *H*-band images, the residuals from the fits indicate that the isoplanatic assumption should be relaxed, and the final model is a faint common Gaussian shape beneath a variable Lorentzian core. However, at a separation of 0.″4, the A and Aa components are forced to follow the strict isoplanatic assumption and have exactly the same PSF shape, just as was the case in the *H*-band analysis. Data obtained from PBD of this image are also given in Table 1.

The relative magnitude errors in Table 1 are perhaps unrealistically low, since they only come from the fitting errors. We would not disagree that they may be 2–3 times greater, but without information external to the experiment, any arbitrary increase in uncertainties at this point would be capricious. Perhaps more realistic relative magnitude uncertainties at various wavelengths are derived from other observations in the sections that follow below.

2.3. *PBD, IBD, and the Isoplanatic Assumption*

In addition to PBD, we also ran the FITSTARS (ten Brummelaar et al. 2000) version of iterative blind

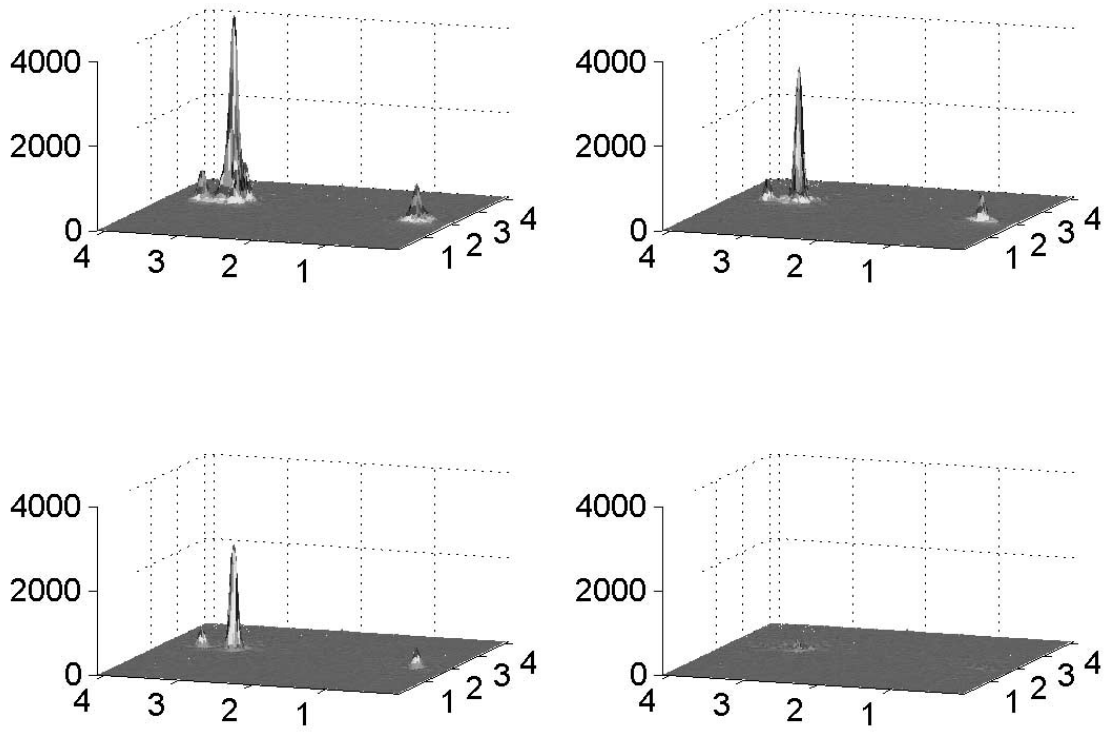

FIG. 3.—Mesh plot of ι Cas at the *H* band showing components A, Aa, and B. *Top left*: Sky-subtracted image. *Top right*: Image with the four-Gaussian aberration pattern subtracted. *Bottom left*: Both the aberration and the Lorentzian core subtracted. *Bottom right*: Aberration, Lorentzian cores, and Airy components subtracted from the image, leaving the residuals. The horizontal axes are in arcseconds, and the vertical axes show counts.

deconvolution (IBD) on the data. IBD forces all stars to have the same shape and structure, but unlike PBD, it does not employ analytic functions and therefore does not produce fitting uncertainties in the end. When both PBD and IBD were initially used under the strict isoplanatic assumption, they gave very similar results for the component magnitude differences in the *H* band, agreeing to within 0.02 mag. In the *I* band, PBD and IBD agree on component magnitude differences to within 0.12 mag for pairs that do not involve the small close companion Aa, but IBD indicated that there was a much greater magnitude difference (3.24) between A and Aa than PBD found (3.00). We offer no explanation for this and are still trying to understand the reason for this discrepancy in one band only. However, it is clear that not all of the stars in the images are within an isoplanatic patch. Since the current FITSTARS IBD method only compares two stars at a time and has no way to relax the strict isoplanatic assumption, it can only really be applied to A-Aa. PBD can be applied to all stars simultaneously, and, as noted above, can be altered to allow some of the functions that comprise the PSF to vary for each star.

We adopt the PBD results in which the A-Aa pair follows the strict isoplanatic assumption, but B and C are allowed to relax. Since only the A-Aa pair is measured under the strict isoplanatic assumption by both IBD and PBD, we can compare the results for only this pair, where again we find a large unexplained discrepancy in the *I* band only. In the *H* band, PBD finds a magnitude difference of 2.00 ± 0.01 (Table 1) compared to 2.03 from IBD. In the *I* band, however, PBD finds 2.89 ± 0.02 and IBD finds 3.24, a discrepancy of 0.35 mag that we cannot explain at this time. While the PBD errors are small in Table 1, the *I*-band IBD result for the A-Aa pair should be kept in mind.

TABLE 1
ι CAS OBSERVATIONAL MEASUREMENTS

Components	Position Angle (deg)	Separation (arcsec)	Magnitude Difference
H Band (J2001.563 = B2001.565)			
A-Aa	71.9 ± 1.0	0.405 ± 0.001	2.00 ± 0.01
A-B	230.5 ± 1.0	2.755 ± 0.010	0.96 ± 0.04
I Band (J2002.140 = B2002.142)			
A-Aa	66.3 ± 1.2	0.414 ± 0.008	2.89 ± 0.02
A-B	228.7 ± 1.2	2.729 ± 0.052	1.44 ± 0.03
A-C	114.3 ± 1.2	7.293 ± 0.138	2.26 ± 0.24

3. ORBITS

The seven speckle measurements listed in the Washington Double Star Catalog (WDS), combined with the two position angles and separations obtained between A and Aa from our images, lead to the first relative orbit for this system, given in Table 2 (solution 3, A-Aa) with a small 0.″007 standard error (Se) of fit. Heintz (1996) combined spectroscopic and positional measurements of the system to derive true orbits for A and B around the center of gravity of A-Aa, but he did not derive a relative orbit. Although he maintained that the orbit of B was "still practically indeterminate," he listed two long-period orbits of 620 and 870 yr, and his preferred 620 yr orbit is given in Table 2. He also adopted an eccentricity of 0 for the orbit of A, since a small eccentricity was indicated.

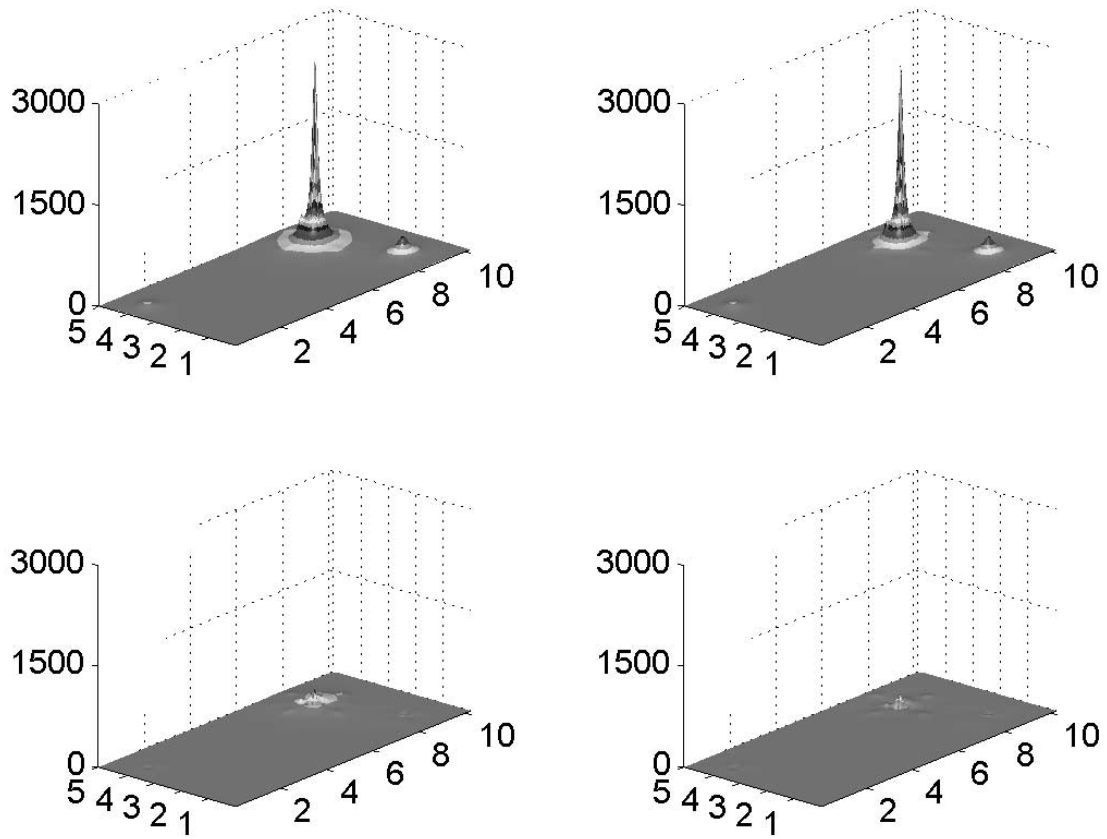

FIG. 4.—Mesh plot of ι Cas at the *I* band showing components A, Aa, B, and C. *Top left*: Sky-subtracted image. *Top right*: Image without the common broad Gaussian (leaving the Lorentzian components). *Bottom left*: Complement image, without the Lorentzian cores (showing the broad Gaussian component). *Bottom right*: PBD model subtracted from the image, leaving some residuals around A and Aa but very little around B and C. The horizontal axes are in arcseconds, and the vertical axes show counts.

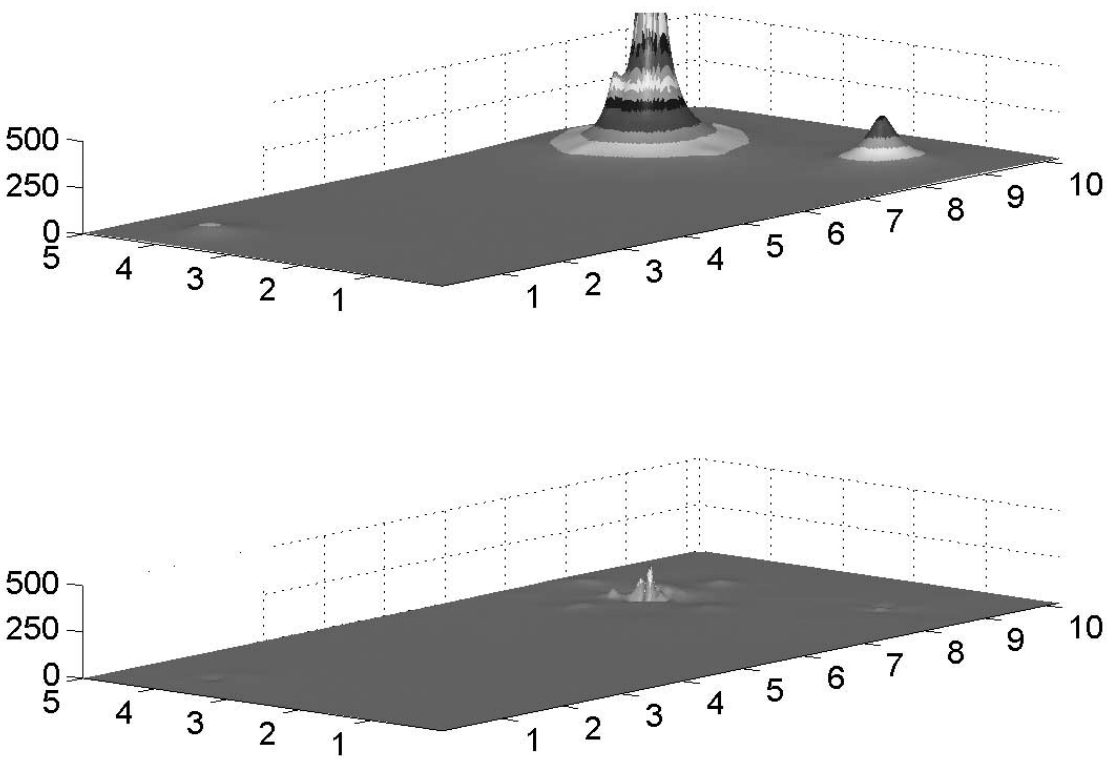

FIG. 5.—Close-up mesh plot of ι Cas at the *I* band. At top the small Aa component sits on the shoulder of A, illustrating the need to account for overlapping PSFs, as is done in PBD. The residuals, image minus model, are shown at the bottom.

TABLE 2
ORBITS

Component	T_0	P (yr)	a (arcsec)	e	ω	Ω	i
Heintz							
A.....	1975.6	49.6	0.107	0	0	148	138
B.....	1640	620	2.88	0.75	283	0.8	115
This paper, solution 1:[a] Se = 0.″12							
A.....	1998.6 ± 8.4	49.67 ± 0.91	0.118 ± 0.015	0.179 ± 0.197	213.8 ± 65.2	204.9 ± 18.1	136.2 ± 12.3
A-Aa.....			...		33.8 ± 65.2		
This paper, solution 2:[b] Se = 0.″095							
A.....	1993.25 ± 0.28	49.50 ± 0.44	0.127 ± 0.013	0.637 ± 0.017	152.8 ± 13.0	181.0 ± 12.3	148.1 ± 6.5
A-Aa.....			0.430 ± 0.022		332.8 ± 15.2		
This paper, solution 3:[c] A-B Se = 0.″14; A-Aa Se = 0.″007							
A.....	1993.22 ± 0.07	47.05 ± 2.02	0.107 ± 0.013	0.626 ± 0.014	148.3 ± 4.3	176.7 ± 4.1	149.2 ± 1.8
A-Aa.....			0.417 ± 0.010		328.3 ± 4.3		

[a] Simultaneous fit of A-B motion for true orbit of A and linear motion of B.
[b] Simultaneous fit for relative orbit of A-Aa, true orbit of A, and linear motion of B.
[c] Sequential fit, first for relative orbit of A-Aa, and then for true orbit of A and linear motion of B.

While the nine recent direct measurements of A and Aa yield the first relative A-Aa orbit, they do not give the semimajor axes of the true orbits for the two components. (All of the other orbital elements are the same for the true orbits of Aa and A, except that A's ω differs by 180° from the relative orbit.) In order to obtain the true semimajor axes, which would then lead to their masses, the amplitude of the oscillations in the relative positions between A and B, or the fourth component C, needs to be determined. This is how Heintz determined the semimajor axis for the true orbit of A. However, all of our attempts failed to find a simultaneous solution for the true and relative orbits of all three components, even though all three components have now been detected and followed. Instead, it is pointed out that the motion of B is so close to linear that it indeed may not be orbitally bound to A, or at any rate it suffices to assign linear motion to B. Thus, we make a simultaneous fit (Table 2, solution 1) for the rectilinear motion of B and the true orbit of A that produces the wobble in the A-B relative motion. By ignoring the relative A-Aa orbit with this method, we find elements similar to Heintz's, including a small eccentricity with a large error.

Also listed in Table 2 is a simultaneous fit (solution 2) for all quantities, obtained by weighting the nine detections of Aa the same as the 193 measurements of B (191 from the WDS and two from us). This results in giving each of the Aa measurements a relative uncertainty of $\sigma = 0.2$ compared to $\sigma = 1$ for each of the B measurements. Since the weight of an observation is proportional to $1/\sigma^2$, the speckle and AO detections of Aa have a weight of 21 times the (mostly visual) measurements of B, in line with the method of the Center for High Angular Resolution Astronomy authors, e.g., Mason, McAllister, & Hartkopf (1995). This solution not only gives the relative orbit but yields much lower uncertainties for the true orbit than does solution 1.

However, by first independently determining the relative orbit from the nine measurements of Aa (step 1) and then using the 193 measurements of B with respect to A to simultaneously find the linear motion of B and the wobble produced on it by a scaled-down relative orbit (step 2), we can lower the uncertainties of the orbital elements even further. The results from this process (solution 3) are designated "sequential" in Table 2, because they are obtained from two successive least-squares fits to the data, the first being a nonlinear least-squares fit to the nine measurements of Aa with respect to A that determines the relative orbital elements, and the second being a linear least-squares fit that determines the true semimajor axis of A and the linear motion of B. The sequential fit is equivalent to giving all of the weight for the orbital elements (except for the size of the A semimajor axis) to the nine-point relative orbit results.

Although the period is better determined from the simultaneous fit, all of the other elements are more accurately determined from the sequential method. Therefore, we adopt all of the elements from the sequential solution 3, and contrary to Heintz, we find a moderate eccentricity orbit. Otherwise, his period is the same as ours, and his inclination and node direction differ from ours by 13° and 28°, respectively. Using the results from the sequential fit, Figure 6 shows the relative orbit for A-Aa, Figure 7 illustrates the motion of Aa and B with respect to A, and Figure 8 depicts the motion of all components with respect to the A-Aa center of mass.

The linear motion of B with respect to the A-Aa center of gravity is the same from either the simultaneous or the sequential fit:

$$B_X = 20.1 \pm 0.5 - 0.0109 \pm 0.0002 \text{ yr},$$

$$B_Y = -1.8 \pm 0.5 - 0.0002 \pm 0.0002 \text{ yr}$$

in Cartesian coordinates (arcseconds), where the year is the decimal year, e.g., 1829.7. Thus, the straight-line motion of B with respect to the A-Aa center of gravity is 10.9 ± 0.2 mas yr^{-1} to the south and 0.2 ± 0.2 mas yr^{-1} to the west. Using the predicted motion of A in 1991.25, the motions of B with respect to A on this date were 24.3 mas yr^{-1} to the south and 3.7 mas yr^{-1} to the east. The *Hipparcos* catalog lists proper motion to the south for B of 8.3 ± 5.8 (or 45 mas

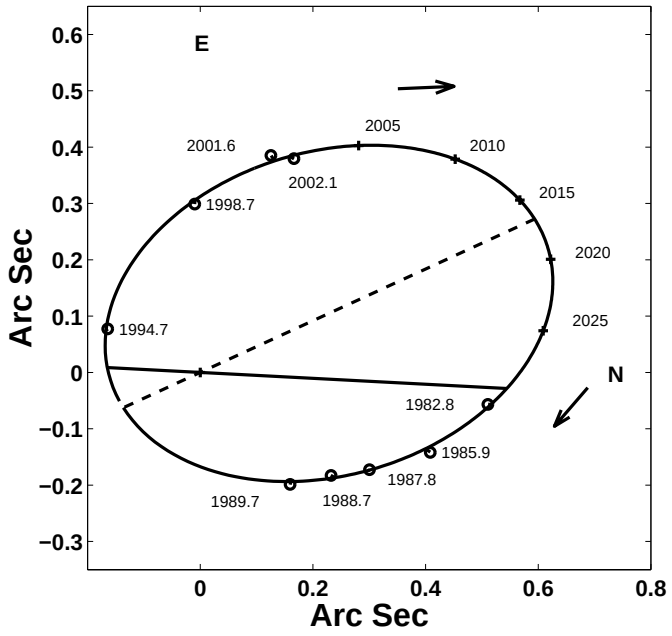

FIG. 6.—Relative orbit of A-Aa. Positions from seven speckle measurements and our two images (the latest two circles) are connected to their predicted positions. The dashed line shows the line of apsides, the solid line shows the line of nodes, and the plus signs indicate future positions.

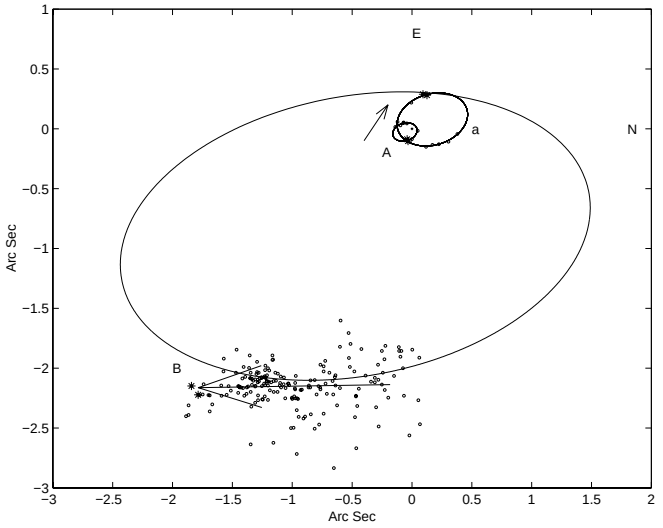

FIG. 8.—Orbits and motion of ι Cas centered on the A-Aa center of gravity. The two inner ellipses show the motion of components A and Aa around their mutual center of gravity (*small plus sign*), along with recent speckle and AO positions. With the suborbital motion of A-Aa subtracted out, the positions of B with respect to the A-Aa center of gravity are shown as small circles along the outer ellipse, which depicts the Heintz's long-period orbit for B. Using the same true orbit for A but linear motion for B results in the arrow at bottom, which begins at the time of the first observation in 1829.7 and ends at 2002.1.

with respect to A) and 48.2 ± 12.8 to the west (or 23 mas to the east with respect to A), all summarized in Table 3. However, *Hipparcos* values must surely be influenced by the orbital motions of A-Aa. In fact, a third orbit for A-Aa (Söderhjelm 1999) derived from a simultaneous solution for *Hipparcos* orbital and proper motions together is certainly not correct ($P = 52$, $T_0 = 1980$, $a = 0.7$, $e = 0.30$, $\omega = 156$, $\Omega = 175$, $i = 106$), especially since it leads to a total mass of $10\ M_\odot$ for the A-Aa-B system.

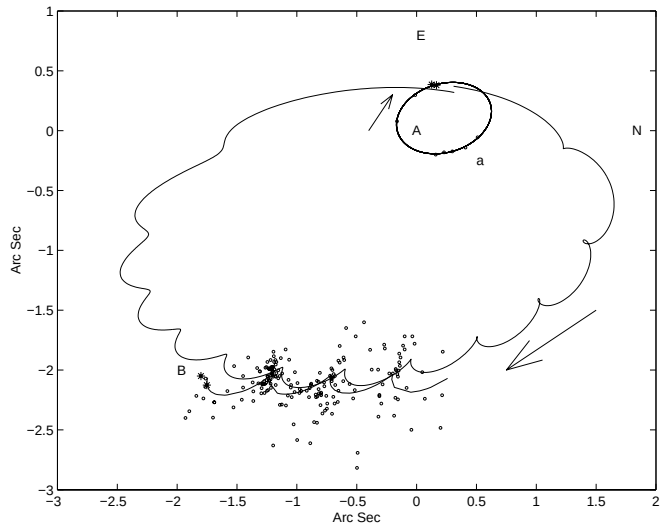

FIG. 7.—Orbits and motion of ι Cas centered on A. With the zero point at component A, i.e., with the letter A plotted at [0, 0], the inner ellipse shows the relative motion of Aa around A, the seven recent speckle positions are indicated by small circles, and our AO positions by asterisks. The positions of B with respect to A are shown as small circles (or asterisks for our AO position) along the long wavy outer line, which depicts the motion of component B around A using our new true orbit for A and Heintz's long-period orbit for B. Using the same true orbit for A but linear motion for B results in the shorter wavy line.

4. MASSES

Because both a true and relative orbit for the A-Aa pair have been obtained and because *Hipparcos* has obtained a good parallax for the system, $\pi = 0\farcs02304 \pm 0\farcs00080$, the masses can be found from the periods and semimajor axes using Kepler's third equation:

$$M_{\rm A+Aa} = \frac{(a_{\rm rel}/\pi)^3}{P^2}\ ,$$

$$M_{\rm Aa} = \frac{(a_{\rm rel}/\pi)^3}{P^2}\frac{a_{\rm true}}{a_{\rm rel}}\ ,$$

$$M_{\rm A} = M_{\rm A+Aa} - M_{\rm Aa}\ .$$

Table 4 gives the masses for solutions 2 and 3, where their errors are propagated from the errors (and covariances) in Table 2 and the parallax error. The masses of the A and Aa components agree quite well with the masses suggested by Heintz: 2.2 and 0.65, respectively, although we find A to be a little lower and Aa a little higher.

TABLE 3
LINEAR MOTION OF B

CASE	MOTION (0″.001 yr^{-1}) East	North
B wrt A+Aa	-0.2 ± 0.2	-10.9 ± 0.2
B wrt A (1991.25)	+3.7	−24.3
B (*Hipparcos*, pm)	-48.2 ± 12.8	-8.3 ± 5.8
B wrt A (*Hipparcos*)	+23.3	−45.4

TABLE 4
MASSES

Component	Solution 2	Solution 3
M_A	1.87 ± 0.39	1.99 ± 0.28
M_{Aa}	0.78 ± 0.15	0.69 ± 0.12
M_{A+Aa}	2.65 ± 0.49	2.68 ± 0.30

5. PHOTOMETRY AND SPECTRAL CLASSIFICATION

No previous magnitude estimates of Aa have been reported, but Johnson band magnitudes, derived from Tycho-2 (Fabricius et al. 2002) magnitudes, are listed in Table 5 for A+Aa and B, marked by footnote a. Even without magnitude differences between A and Aa at any other wavelength but ours at *I* and *H*, it is still possible to address many quantities of astrophysical interest by using the B component's F5 spectral classification from the Tycho catalog as a reference. Figure 9, constructed with data from Allen (1983) and Zombeck (1990), shows the main sequence in four bands, with component B placed in the diagram by using the *Hipparcos* distance of 43.4 ± 1.5 pc for the A-B system, its Tycho magnitudes (*large filled symbols*) listed in Table 5, and its temperature derived from the Tycho $B-V$ color index. The smaller open circles in Figure 9 are its projected magnitudes at the *I* and *H* bands using the colors appropriate to the $B-V$ temperature. From its position just below the main sequence and from the decoupling of the motions of A and B in § 3, the B component may not be at the same distance as A but may instead be at 50 pc, corresponding to the 0.31 mag increase required to place it on the main sequence.

Assuming that the other stars lie precisely on the main sequence, then by combining the *Hipparcos* distances with the apparent magnitude differences at *I* and *H* between the rest of the components and B, we can plot them on the *I* and *H* main sequence as larger open symbols. Component Aa appears to be G5 in the *H* band or G7 from the *I*-band results, and A appears to be A7 at *H* or A4 at *I*. With the Johnson *B* and *V* combined magnitudes derived from the Tycho-2 catalog (footnote a in Table 5) as a constraint, we can use either component's temperature from Figure 9 to project its magnitude to *B* and *V* and then derive the other component's magnitude, temperature, and spectral type. These projections are shown on the main sequences as smaller open symbols. However, using component A to derive Aa properties results in a much larger spread across Figure 9 for Aa than the converse does for A. Therefore, we use the position of Aa to derive the position of A and find that most of the points fall around A3. We thus adopt a spectral type of A3 for component A, but with increasing cooler types implied at increasing wavelengths. Component Aa appears to be G6. No previous separate spectral observations for A or Aa exist, but A+Aa is in the Tycho catalog as a low-amplitude α CVn variable, spectrum-variable, A5p strontium star.

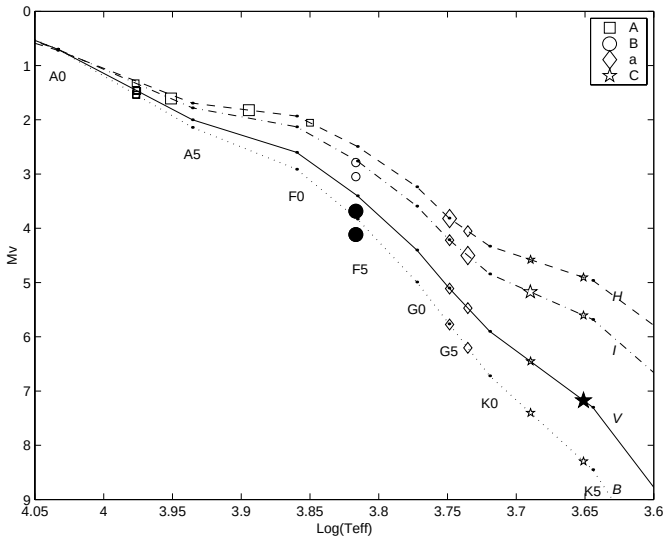

FIG. 9.—Absolute magnitude vs. effective temperature at different wavelengths. From top down, lines depict the main sequence at the *H*, *I*, *V*, and *B* bands, with each spectral class indicated by a vertical series of dots. Based on the B component, the absolute Tycho magnitudes are plotted as large filled symbols. Our *I* and *H* magnitude differences (from Table 1) for the other components with respect to B are plotted with large open symbols at the intersection with the appropriate main sequence. Small open symbols indicate a magnitude determined from an observation made at a different wavelength and projected with the appropriate temperature. The positions on the *B* and *V* main sequence for component A are determined from the Tycho combined A+Aa *B* and *V* magnitudes and from our determinations of the *B* and *V* magnitudes of Aa.

Hipparcos finds that component C is closer (23.7 ± 6.5 pc) than A+Aa and B. Placing it on the *I*-band main sequence in Figure 9 with this distance and its *I* magnitude,

TABLE 5
BVIH APPARENT MAGNITUDES

		MAGNITUDE			
COMPONENT	SPECTRAL CLASS	*B*	*V*	*I*	*H*
A+Aa	A5p	4.707 ± 0.021[a]	4.618 ± 0.015[a]	4.58 ± 0.20[b]	4.97 ± 0.16[b]
A	A3	4.73 ± 0.01[c]	4.65 ± 0.01[c]	4.65 ± 0.20[b]	5.13 ± 0.16[b]
B	F5	7.30 ± 0.02[a]	6.87 ± 0.02[a]	6.24[d]	5.97[d]
C	K3	9.7 ± 0.6[d]	8.7 ± 0.5[b]	7.3 ± 0.3[b]	6.6 ± 0.2[d]
Aa	G6	9.2 ± 0.2[d]	8.48 ± 0.25[d]	7.55 ± 0.20[b]	7.12 ± 0.16[b]

[a] Johnson magnitude converted from Tycho-2 B_T and V_T.
[b] Magnitude projected from another wavelength and from our measured magnitude difference with respect to *B* (or the Hipparcos *V* magnitude for the C component).
[c] Magnitude from our results for component Aa and from the A+Aa combined magnitude.
[d] Magnitude from colors of adopted temperature and magnitudes at other wavelengths.

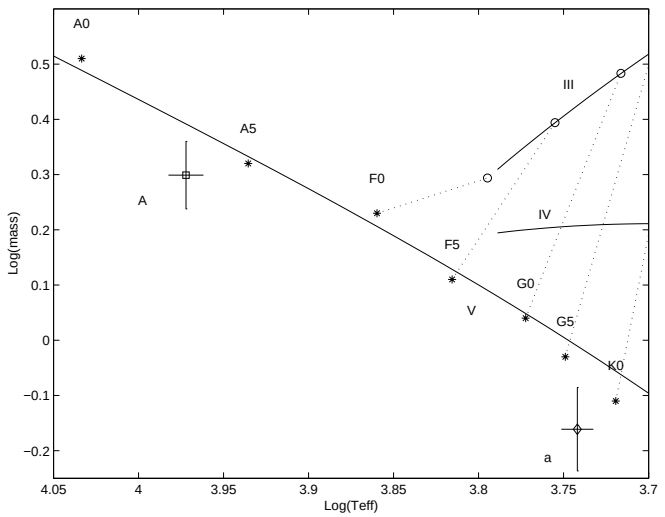

FIG. 10.—Mass vs. effective temperature. Luminosity classes are marked as lines III, IV, and V, and spectral classes are indicated. The masses of components A and Aa are plotted with vertical bars indicating their mass uncertainty. The horizontal error bars come from ambiguities in the spectral classification from Fig. 9.

derived from the B − C magnitude difference in Table 1 and the *I* magnitude of B from Table 5, we find it to be a K2 star at *I*. Although Heintz reports a *V* magnitude of 8.4 for C, Tycho gives a *V* magnitude of 9.05 ± 0.06, plotted as the filled star in Figure 9. This position in Figure 9 indicates that C may be a K5 star. Taken together, we adopt a K3 classification for C, with large uncertainties in its properties as given in Table 5.

In summary, except for component B, each component is required to lie on the main sequence in Figure 9, and except for the large–filled-symbol Tycho magnitudes (footnote a in Table 5), all magnitudes are either based on B directly (*large open symbols*) or projected from an observation at another wavelength (*small open symbols*). The *B* and *V* magnitudes (*small open symbols*) of A are from the projected *B* and *V* magnitudes of Aa and the Tycho-2 combined A+Aa magnitudes. A careful inspection of Figure 9 reveals that every star has two points on each main sequence. Table 5 lists the average and range for each pair of points at each wavelength.

Using the mean of the two temperatures for Aa illustrated in Figure 9, and six of the eight for component A (excluding its *H* temperatures), we plot their temperatures against their masses derived from solution 3 in § 4 and notice in Figure 10 that their masses are a little low for their spectral types. Considering that a full orbital revolution has not been observed, the masses may yet end up on the main sequence, although even now they are not unreasonable.

6. SUMMARY

With adaptive optics images taken at the AEOS 3.63 m telescope on Haleakala, we have obtained relative photometry of components of ι Cas at *I*- and *H*-band wavelengths, taking into account the fact that the images were not obtained through an isoplanatic patch. The *H*-band image is the first to show the Aa component 0.″4 from A (although it has been resolved with speckle interferometry), which leads to the first reported relative photometry between the two: a magnitude difference of 2.0. The *I*-band image is the first is to show four components in the system, from which we find a magnitude difference of 2.9 between A and Aa. Combining our photometry with *B*- and *V*-band data from the Tycho catalog and assuming that the four stars are relatively normal main-sequence stars, the relative photometry leads to spectral types of A3, F5, K3, and G6 for components A, B, C, and Aa, respectively.

We have decoupled the motion of component B from the A-Aa pair (which leaves only two of the four components in the system as physically related) and have derived the latter's true and relative orbits. From the distance and orbit, masses of 1.99 and 0.69 $M_{\odot}$ are derived for A and Aa, respectively, both lower than expected for zero-age main-sequence stars of their spectral types.

The ι Cas system is good for studying the effects of non-isoplanatism on photometry with adaptive optics because there are four stars within 7.″3, including a very close pair at 0.″4.

We thank two anonymous referees for thorough reviews and the editor for an equitable and fair handling of the manuscript. We are very grateful to Haosheng Lin at the Institute for Astronomy at the University of Hawaii for allowing us to borrow the NICMOS camera. Support at the AEOS facility from the staff of the Maui Space Surveillance System on Haleakala is greatly appreciated. This research was supported by the Air Force Office of Scientific Research, with thanks to Paul Bellaire. L. C. R. received funding from Boeing under AFRL/DE contract F29601-00-D-0204. With personal assistance from Gary Wycoff, data for this paper came from The Washington Double Star Catalog as maintained by Brian Mason and the staff at the United States Naval Observatory. Data from *Hipparcos* can be obtained at its Web site[2] or can be found in the 1997 publication ESA SP-1200, the Hipparcos and Tycho Catalogs. The Tycho-2 Catalog is also available on-line.[3] This research has also made use of NASA's Astrophysics Data System.

[2] See http://astro.estec.esa.nl/Hipparcos/catalog.html.
[3] See http://cdsweb.u-strasbg.fr/cgi-bin/qcat?.

REFERENCES

Allen, C. W. 1983, Astrophysical Quantities (3d ed.; London: Athlone)
Barnaby, D., Spillar, E., Christou, J. C., & Drummond, J. D. 2000, AJ, 119, 378
Drummond, J., Milster, S., Ryan, P., & Roberts L. 2002, Proc. SPIE, 4839, in press
Drummond, J. D. 1998, Proc. SPIE, 3353, 1030
Fabricius, C., Høg, E., Makarov, V. V., Mason, B. D., Wycoff, G. L., & Urban, S. E. 2002, A&A, 384, 180
Heintz, W. D. 1996, AJ, 111, 408
Mason, B. D., McAlister, H. A., & Hartkopf, W. I. 1995, AJ, 109, 332
McAlister, H. A., Hartkopf, W. I., Hutter, D. J., & Franz, O. G. 1987, AJ, 93, 688
Roberts, L. C., & Neyman, C. R. 2002, PASP, 114, 1260
Ryan, P. T., Drummond, J. D., & Milster, S. 2002, Proc. SPIE, 4860, in press
Ryan, P. T., Fugate, R. Q., Angel, J. R. P., McCarthy, D. W., Mohanty, S., & Sandler, D. G. 1998, Appl. Opt., 37, 7035
Söderhjelm, S. 1999, A&A, 341, 121
ten Brummelaar, T., Mason, B. D., McAlister, H. A., Roberts, L. C., Turner, N. H., Hartkopf, W. I., & Bagnuolo, W. G. 2000, AJ, 119, 2403
Zombeck, M. V. 1990, Handbook of Space Astronomy and Astrophysics (2d ed.; Cambridge: Cambridge Univ. Press)